Oxidation of di-n-butyl ether: Experimental characterization of low-temperature products in JSR and RCM

Nesrine Belhadj, Roland Benoit, Philippe Dagaut, Maxence Lailliau, Zeynep Serinyel, Guillaume Dayma, Fethi Khaled, Bruno Moreau, Fabrice Foucher

Oxidation of di-n-butyl ether: Experimental characterization of low-temperature products in JSR and RCM

Nesrine Belhadj[1,2], Roland Benoit[1], Philippe Dagaut[1,*], Maxence Lailliau[1,2], Zeynep Serinyel[1,2], Guillaume Dayma[1,2]

[1] CNRS–INSIS, ICARE, 1C avenue de la Recherche Scientifique, 45071 Orléans cedex 2, France

[2] Université d'Orléans, rue de Chartres, 45100 Orléans, France

Fethi Khaled[3], Bruno Moreau[3], Fabrice Foucher[3]

[3]PRISME, Université d'Orléans, rue de Chartres, 45100 Orléans, France

*Corresponding author:

Philippe Dagaut

CNRS–ICARE, Institut de Combustion, Aérothermique, Réactivité et Environnement

1C Avenue de la Recherche Scientifique

45071 Orléans Cedex 2, France

Tel: +33 (0)2 38 25 54 66

dagaut@cnrs-orleans.fr

Abstract

The oxidation of di-n-butyl-ether (DBE) was performed in a jet-stirred reactor (JSR) at 1 atm, 520 and 530 K, and from 480 to 670 K at10 atm, at a residence time of 1 s, an equivalence ratio of 0.5, and an initial fuel concentration of 5000 ppm. Ignition experiments on DBE/air mixtures were also performed in a rapid compression machine (RCM) under stoichiometric conditions, 5 bars, and from 550 to 630 K. Low-temperature products formed in JSR and RCM experiments were characterized. To this end, high-resolution mass spectrometry analyses (HRMS) with flow injection analyses or ultra-high pressure liquid chromatography coupling were used to characterize hydroperoxides and diols ($C_8H_{18}O_3$), ketohydroperoxides ($C_8H_{16}O_4$), carboxylic acids ($C_2H_4O_2$, $C_3H_6O_2$, $C_4H_8O_2$), di-keto ethers ($C_8H_{14}O_3$), and highly oxygenated molecules ($C_8H_{14}O_5$, $C_8H_{16}O_6$, $C_8H_{14}O_6$, $C_8H_{14}O_7$, $C_8H_{16}O_8$, and $C_8H_{14}O_9$) resulting from up to five O_2 additions on fuel's radicals. Whereas HOMs are of minor importance in combustion, they are considered key species for the formation of secondary organic aerosols. In addition, cyclic ethers and esters ($C_8H_{16}O_2$) were observed. Heated electrospray and atmospheric pressure chemical ionizations (HESI and APCI) were used in positive and negative modes for MS analyses. H/D exchange with D_2O was used to confirm the presence of –OH or –OOH groups in the products. The present results show that DBE oxidation proceeds similarly under JSR and RCM conditions. Whereas the CH_2 groups neighboring the ether group are the most favorable sites for H-atom abstraction reactions, speciation indicated that other sites can react by metathesis forming a large pool of intermediates and products. Our kinetic reaction mechanism needs to be extended for simulating the formation of newly detected species.

Keywords: dibutyl ether, jet-stirred reactor, rapid compression machine, cool flame, ketohydroperoxides, highly oxygenated molecules.

1. Introduction

The interest for alternative transportation biofuels is still growing. Among them, aliphatic ethers, which can be produced through dehydration of alcohols, are of particular interest. Recently, the kinetics of oxidation of C_4 to C_8 aliphatic ethers received particular attention [1-10] and some of their low-temperature products have been characterized. Indeed, their high reactivity favors the analysis of hydroperoxides (ROOH), ketohydroperoxides (KHP) [11-19] formation and recently proposed new oxidation pathways [20, 21] leading to highly oxygenated molecules (HOMs) which are considered minor combustion products. However, in the troposphere they are considered of paramount importance for the formation of secondary organic aerosols [22]. Chromatographic separation of ketohydroperoxides, formed by oxidation of large hydrocarbons, and detection by UV absorption or mass spectrometry has been attempted in the past [11-19], but was technically limited. Nowadays, with more powerful analytical techniques such as synchrotron based mass spectrometry[21, 23, 24], ultra-high pressure liquid chromatography and high-resolution mass spectrometry (Orbitrap®), one can expect improving the characterization of low temperature oxidation products[25].

Therefore, new experiments were performed in a JSR and an RCM to characterize di-n-butyl ether (DBE) low temperature oxidation products. Among them, hydroperoxides, ketohydroperoxides, carboxylic acids, and highly oxygenated molecules resulting from multiple O_2 addition on fuel's radicals were tracked using soft chemical ionization and high-resolution mass spectrometry. Because our chemical kinetic model for the oxidation of DBE

[9] could represent experimental results obtained for stable products, we used it to simulate the global formation of ketohydroperoxides under JSR conditions.

2. Experimental

Two complementary experimental techniques were employed in this work to characterize the products of DBE oxidation, namely a jet-stirred reactor (JSR) and a rapid compression machine (RCM). Table 1 summarizes the present experimental conditions in JSR and RCM.

Table 1. Experimental conditions

JSR		RCM
Equivalence ratio (φ): 0.5 Reactive mixture: 0.5% of DBE, 12% O_2, 87.5% N_2 Residence time: 1 s Pressure:		Equivalence ratio (φ): 1 Reactive mixture: DBE/air, 21% O_2, 79 % N_2 Compression time ($p_{max}/2$ to p_{max} (t_{50}) < 4 ms Pressure: 5 bar
10 atm	1 atm	
Temperature: 480 to 670 K	520 and 530 K	Temperature: 550 to 630 K

2.1 JSR

Experiments were performed in a fused silica jet-stirred reactor setup already described in details [26] and used earlier [27, 28]. As in previous works [9, 28] the liquid fuel (>99% pure from Sigma Aldrich) was atomized by a nitrogen flow and vaporized in a heated chamber. The fuel and oxygen were sent separately to the JSR to avoid oxidation before reaching the 4 injectors (nozzles of 1 mm I.D.) providing stirring. Flow rates of the nitrogen diluent and oxygen were controlled by mass flow meters. The liquid fuel was pumped using an HPLC pump (Shimadzu LC10 AD VP) with an online degasser (Shimadzu DGU-20 A3). Good thermal homogeneity along the vertical axis of the JSR was recorded (gradients of < 1 K/cm) by thermocouple measurements (0.1 mm Pt-Pt/Rh-10% wires located inside a thin-wall silica tube). A low-pressure sonic probe was used to freeze the reactions and take samples for off line analyses. In order to measure low-temperature products e.g., cyclic ethers, diols, hydroperoxides, ketohydroperoxides (KHPs), di-ketohydroperoxides, keto-di-hydroperoxides, and other highly oxygenated products, the sonic probe samples were bubbled into cooled acetonitrile (at 1 atm: 0°C, 250 mL, 90 min; at 10 atm: 0°C, 25 mL, 75 min). The resulting solution was stored in a freezer at -15°C for further chemical analyses.

2.2 Rapid Compression Machine

The RCM is an experimental facility that allows rapid compression of a gaseous mixture (DBE/air mixture presently). This rapid compression leads to a fast increase of pressure and temperature of the mixture. For a fuel/air mixture, this increase of pressure and temperature leads to a build-up of chemical reactions that causes ignition after some characteristic time called ignition delay time. This RCM contains a creviced piston to avoid the vortex formation and to ensure the post-combustion charge homogeneity. The use of a creviced piston, which was largely employed in previous experimental works[29-32] helps to study the hydrocarbon autoignition chemistry limiting physical effects. Further details of the RCM of the University of Orléans can be accessed elsewhere [33, 34]only a brief description of this machine is presented here.

(Figure 1)

In-cylinder pressure histories (Fig. 1) are recorded by an AVL QH32C piezoresistive transducer while the intake pressure was followed by a Keller PAA-33X/80794, the sensor is protected as recommended in [35]. The gas preparation reservoir temperature and piston initial temperature were measured by K-type thermocouples. The gas mass flow rates were regulated by Bronkhorst Cori-flow M13. The errors of measurement of in-cylinder pressure, intake pressure, intake temperatures, and mass flow rate are ± 1%, ± 1 mbar, ± 2 K and ± 1% respectively. To obtain the right equivalence ratio, the gaseous fuel was premixed with the synthetic air from Air Liquide in a reservoir at 3 bar. Before the preparation of mixtures, the reservoir was cleaned by flux of air and then pumped out to reach vacuum condition (< 1 mbar), which ensured no compound accumulated in the reservoir. The weight of the liquid fuel introduced into the reservoir was determined as the difference in the weight of the syringe before and after the

introduction. The temperature of the reservoir was maintained at 80 °C to ensure the total vaporization of the liquid fuels. For each gas mixture, a mechanic agitation during 30 minutes was conducted to ensure the homogeneity. All gas mixtures were prepared on the day of manipulation. For each measurement, the pressure at the top dead center (P_c) and the temperatures at top dead center (T_c) were obtained by regulating the intake pressure and the piston initial temperature. The T_c are calculated thanks to the isentropic relation, where γ is the ratio of specific heats of gas mixture:

$$\int_{T_0}^{T_c} \frac{\gamma}{\gamma - 1} \frac{dT}{T} = ln\left(\frac{P_c}{P_0}\right) \quad (1)$$

In order to analyze the composition of the mixture after build-up of chemical reactions, but before the actual time of ignition samples, were taken. For each RCM run, a sampling orifice located at the endwall of the RCM is opened at a preset time and the gas of the combustion chamber is evacuated and stored inside a pre-vacuumed sampling tank. If many runs are to be sampled in the same tank, the tank is vacuumed only before the first run and then additional runs are accumulated in the tank. The sample accumulated in the sampling tank is then kept inside a freezer at a temperature of -30°C before dissolution in ACN for chemical analyses.

2.3 Chemical analyses of low-temperature products

Mass spectrometry (MS) analyses were performed by flow injection (flow of 5-8 µL/min recorded for 1 min for data averaging) in the ionization chamber of an Orbitrap® Q-Exactive mass spectrometer (mass resolution of 140,000 and mass accuracy <1 ppm RMS) and ultra-high-pressure liquid chromatography-MS (UHPLC-MS). Ionization settings in FIA were: sheath gas flow of 8-15 a.u., auxiliary gas flow of 0 a.u., sweep gas flow of 0 a.u., capillary temperature of 220-250°C, vaporizer temperature of 80-100°C, corona discharge current of 2 µA, spray voltage of 3.8 kV. Mass calibrations were performed using commercial ESI positive and negative calibration mixtures (Thermo Scientific) in flow injection mode (FIA).

UHPLC-MS analyses were performed using an analytical column (C_{18} Phenomenex Luna, 1.6µm, 100 Å, 100x2.1 mm) for products separation after injection of 3 µL of sample eluted by water-acetonitrile (ACN) (gradient 5% to 90% ACN) at a flow rate of 250 µL/min. Ion Max® heated electrospray ionization (HESI) and atmospheric chemical ionization (APCI) were used in positive and negative modes for the ionization of products. APCI settings were: sheath gas flow of 55 a.u., auxiliary gas flow of 6 a.u., sweep gas flow of 0 a.u., capillary temperature of 300°C, vaporizer temperature of 150°C, corona discharge current of 3 µA. In HESI mode, we used a spray voltage of 3.8 kV. Whereas oxidation of analytes by HESI has been reported previously [36, 37], we verified here that no oxidation occurred in the ion source by injecting a solution DBE-ACN in both HESI and APCI modes.

To determine the structure of cool flame products, MS-MS analyses were performed at collision cell energy of 10 eV. The fast OH/OD exchange [21] was used to verify the presence of hydroxy and hydroperoxy groups in the products. To this end, we added 300 µL of D_2O (99.96% D, ref. 26978-6 from Sigma-Aldrich) to 1.5 mL of sample (reaction time 20 min). The resulting solution was analyzed by mass spectrometry in FIA and HESI mode. UHPLC analyses with D_2O/CAN solvent were also performed.

3. Kinetic modeling

The computations were performed using the PSR computer code [38] from the Chemkin II package[39]. Our kinetic mechanism presented earlier [9] was used. It involves 467 species and 2768 reactions covering both high- and low-temperature chemistry, limited to 2 additions of O_2 to fuel's radicals, which yield ketohydroperoxides. The formation of the most likely KHPs at 520 K during the oxidation of 5000 ppm of DBE at 10 atm and an equivalence ratio of 0.5 is presented in Figure 2. According to the modeling, DBE is mainly consumed through H-atom abstraction by hydroxyl radicals. The resulting fuel radicals undergo peroxidation by reaction with molecular oxygen.

(Figure 2)

Because it was demonstrated earlier that the chemical kinetic model for DBE oxidation [9] represents fairly well our JSR data, it was used to predict newly characterized species, namely ketohydroperoxides. The results are presented in the next section.

4. Results and discussion

The formation of ketohydroperoxides and highly oxygenated compounds resulting from O_2 addition on the fuel's radicals (R) could be observed here in both JSR and RCM experiments. Their formation proceeds through a sequence of reactions: R + O_2 ⇆ RO_2; RO_2 ⇆ QOOH; QOOH + O_2 ⇆ OOQOOH; OOQOOH ⇆ HOOQ'OOH

followed by the formation of the hydroxyl radical and a ketohydroperoxide ($C_8H_{16}O_4$): HOOQ'OOH → HOOQ'O + OH. Dihydroperoxides can also react with molecular oxygen (3rd O_2 addition): HOOQ'OOH + O_2 ⇆ $(HOO)_2Q'OO$; $(HOO)_2Q'OO$ ⇆ $(HOO)_2POOH$; $(HOO)_2POOH$ → OH + $(HOO)_2P{=}O$ ($C_8H_{16}O_6$). The reaction can also proceed through a 4th O_2 addition: $(HOO)_2POOH + O_2$ → $(HOO)_3POO$; $(HOO)_3POO$ ⇆ $(HOO)_3P'OOH$; $(HOO)_3P'OOH$ → OH + $(HOO)_3P'{=}O$ ($C_8H_{16}O_8$). The products of third and fourth oxygen addition were well observed in the present experiments confirming the extended oxidation pathways proposed earlier [21] whereas in a previous JSR study of di-n-pentyl ether oxidation, only products of the third O_2 addition ($C_{10}H_{20}O_6$) could be observed by synchrotron vacuum ultraviolet photoionization molecular beam-time of flight mass spectrometry (SVUV-MB-TOF-MS) [21]. Under JSR and RCM conditions, we could also observe the products of O_2 fifth addition yielding $C_8H_{14}O_9$ at trace level, and the formation of diols and hydroperoxides ROOH (Table 2 and Table 3). It has been proposed that diols derive from the decomposition of di-hydroperoxides [16] whereas hydroperoxides can result from H-atom abstraction by RO_2: $RO_2 + R'H$ → ROOH + R'.

Table 2. Products of DBE oxidation in a JSR at 520 K and 1 atm. H/D exchange by addition of D_2O performed in FIA HESI (+) mode only. Newly observed products are indicated by an asterisk.

MW	Species		HESI (+)		HESI (–)	
(g/mole)	Formula	Name	m/z (+H)	Signal (a.u)	m/z (-H)	Signal (a.u)
58	C_3H_6O	acetone	59.0492	6.1E6	57.0345	4.4E6
60	$C_2H_4O_2$	acetic acid	61.0284	1.3E7	59.0139	1.9E7
61	*$C_2H_3DO_2$*	*acetic acid-d_1**	*62.0347*	*1.0E6*	-	-
62	H_2CO_3	carbonic acid	-	-	60.9932	7.1E5
70	C_4H_6O	butenal	71.0491	1.0E8	69.0346	4.2E5
72	C_4H_8O	butanal	73.0647	1.0E7	71.0502	7.2E6
74	$C_4H_{10}O$	butanol	75.0804	2.2E5	73.0659	4.5E5
75	*C_4H_9DO*	*butanol-d_1**	*76.0867*	*1.0E4*	-	-
74	$C_3H_6O_2$	propanoic acid	75.0441	7.8E6	73.0295	2.6E7
75	*$C_3H_5DO_2$*	*propanoic acid -d_1**	*76.0503*	*1.6E6*	-	-
76	$C_3H_8O_2$	propyl hydroperoxide	77.0596	9.9E4	75.0451	1.1E5
86	$C_4H_6O_2$	γ-butyrolactone#, 2,3-butanedione#	87.0440	7.2E7	85.0295	1.3E7
88	$C_4H_8O_2$	butanoic acid# and isomers	89.0597	7.6E7	87.0452	1.4E8
102	$C_5H_{10}O_2$	butyl formate# and isomers	103.0753	7.7E5	101.0608	3.7E5
116	$C_6H_{12}O_2$	butyl acetate# and isomers	117.0910	1.5E6	115.0764	3.5E5
118	$C_5H_{10}O_3$	butyl hydrogen carbonate*	119.0703	9.7E5	117.0557	6.0E5
144	$C_8H_{16}O_2$	cyclic ethers, butyl butyrate#	145.1222	2.1E7	143.1076	4.0E4
158	$C_8H_{14}O_3$	butyric anhydride# and di-keto ethers	159.1016	1.6E8	157.0869	3.2E6
162	$C_8H_{18}O_3$	ROOH, diols*	163.1328	2.7E7	161.1187	8.6E3
163	*$C_8H_{17}DO_3$*	*ROOD, diols-d_1**	*164.1392*	*1.2E7*	-	-
164	*$C_8H_{16}D_2O_3$*	*diols-d_2**	*165.1454*	*1.5E6*	-	-
176	$C_8H_{16}O_4$	KHP	177.1121	2.7E8	175.0974	2.3E6
177	*$C_8H_{15}DO_4$*	*KHP-d_1*	*178.1183*	*1.2E8*	-	-
190	$C_8H_{14}O_5$	di-keto-ROOH	191.0914	2.2E7	189.0767	6.7E6

191	*$C_8H_{13}DO_5$*	*di-keto-ROOD*	*192.0976*	*1.0E7*	-	-
194	$C_8H_{18}O_5$	di-ROOH*	195.1227	2.7E5	193.1080	1.6E6
195	*$C_8H_{17}DO_5$*	*HOOROOD**	*196.1290*	*7.0E4*	-	-
196	*$C_8H_{16}D_2O_5$*	*DOOROOD**	*197.1349*	*6.9E3*	-	-
206	$C_8H_{14}O_6$	unsaturated keto-di-ROOH*	207.0864	1.7E6	-	-
207	*$C_8H_{13}DO_6$*	*unsaturated keto-di-HOOROOD*	*208.0926*	*8.8E5*	-	-
208	*$C_8H_{12}D_2O_6$*	*unsaturated keto-di-ROOD*	*209.0990*	*9.6E4*	-	-
208	$C_8H_{16}O_6$	keto-di-ROOH	209.1020	4.2E6	207.0873	9.35E6
209	*$C_8H_{15}DO_6$*	*keto-di-ROOH-d_1*	*210.1082*	*2.7E6*	-	-
210	*$C_8H_{14}D_2O_6$*	*keto-di-ROOD*	*211.1145*	*6.3E5*	-	-
222	$C_8H_{14}O_7$	di-keto-di-ROOH	223.0812	8.8E5	221.0666	1.14E7
223	*$C_8H_{13}DO_7$*	*di-keto-HOOROOD**	*224.0875*	*8.3E5*	-	-
224	*$C_8H_{12}D_2O_7$*	*di-keto-DOOROOD**	*225.0937*	*2.1E5*	-	-
240	$C_8H_{16}O_8$	keto-tri-ROOH*	-	-	239.0773	5.12E7
254	$C_8H_{14}O_9$	di-keto-tri-ROOH *	-	-	253.0566	1.75E4

Note: # identification verified by UHPLC-MS-MS of the pure compound in ACN

Table 3. Products of oxidation in a JSR at 560 K and 10 atm and in a RCM at 570K and 5 bar. Analyses were performed by FIA in APCI (+/-) mode only. Newly observed products are indicated by an asterisk.

MW	Species			JSR	RCM		JSR	RCM
(g/mole)	Formula	Name	m/z (H+)	Signal (a.u.)	Signal (a.u)	m/z (-H)	Signal (a.u.)	Signal (a.u)
58	C_3H_6O	acetone	59.0492	2.0E7	4.3E6	57.0345	2.6E8	3.3E7
60	$C_2H_4O_2$	acetic acid	61.0284	2.2E7	7.4E6	59.0139	8.1E7	1.0E8
62	H_2CO_3	carbonic acid	-	-	-	60.9932	1.0E5	2.0E7
70	C_4H_6O	butenal	71.0491	75.3E8	7.0E7	69.0346	1.0E7	2.0E6
72	C_4H_8O	butanal	73.0647	1.6E8	4.5E7	71.0502	1.0E7	4.0E6
74	$C_4H_{10}O$	butanol	75.0804	2.1E4	3.0E5	73.0659	6.9E6	1.0E5
74	$C_3H_6O_2$	propanoic acid	75.0441	7.1E6	1.5E6	73.0295	2.4E7	7.0E7
86	$C_4H_6O_2$	γ-butyrolactone#, 2,3-butanedione#	87.0440	4.5E8	8.9E7	85.0295	4.5E7	1.0E8
88	$C_4H_8O_2$	butanoic acid# and isomers	89.0597	2.8E8	4.0E7	87.0452	9.9E7	1.0E9
102	$C_5H_{10}O_2$	butyl formate# and isomers	103.0753	5.3E6	1.6E6	101.0608	2.7E5	-
116	$C_6H_{12}O_2$	butyl acetate# and isomers	117.0910	9.8E6	1.1E6	115.0764	4.9E5	6.0E6
118	$C_5H_{10}O_3$	butyl hydrogen carbonate*	119.0703	2.7E5	7.8E5	117.0559	3.2E7	2.5E6

144	$C_8H_{16}O_2$	cyclic ethers, butyl butyrate	145.1222	8.5E7	1.3E7	143.1076	4.3E4	5.0E6
158	$C_8H_{14}O_3$	butyric anhydride#, di-keto ethers	159.1016	1.5E9	1.6E8	157.0869	4.9E6	5.0E7
162	$C_8H_{18}O_3$	ROOH, diols*	163.1328	1.3E8	1.5E7	161.1187	3.1E4	1.0E4
176	$C_8H_{16}O_4$	KHP	177.1121	6.8E8	8.64E7	175.0974	1.9E6	6.0E6
190	$C_8H_{14}O_5$	di-keto-ROOH	191.0914	8.3E7	5.9E6	189.0767	5.6E6	6.7E6
194	$C_8H_{18}O_5$	di-ROOH*	195.1227	1.5E5	5.4E5	193.1080	1.7E5	3.0E6
206	$C_8H_{14}O_6$	unsaturated keto-di-ROOH*	207.0864	2.6E6	2.1E5	205.0720	5.7E6	8.9E5
208	$C_8H_{16}O_6$	keto-di-ROOH	209.1020	4.5E5	2.5E6	207.0873	2.1E7	3.0E6
222	$C_8H_{14}O_7$	di-keto-di-ROOH	223.0812	9.1E3	5.9E4	221.0666	1.1E7	6.8E5
240	$C_8H_{16}O_8$	keto-tri-ROOH*	-	-	-	239.0773	1.8E7	5.0E5
254	$C_8H_{14}O_9$	di-keto-tri-ROOH *	-	-	-	253.0566	2.0E6	1.8E4

Note: # identification verified by UHPLC-MS-MS of the pure compound in ACN

The so-called Korcek mechanism [40], through which the γ-ketohydroperoxides key-intermediates are transformed into stable products (acids and ketones), e.g. butanoic acid here (Fig. 3 where the scheme presented follows that of Jalan et al.[40]) can modify the overall system reactivity [41]. The computational work of Grambow et al. [42] showed that from 75 possible unimolecular reaction of C_3 γ-KHP, the Korcek mechanism had the lowest transition state energy. Butanoic acid was observed in the present experiments performed in JSR and RCM (Tables 2 and 3). Besides butanoic acid, other products can be formed via the Korcek mechanism, such as acetone (C_3H_6O) and butyl hydrogen carbonate ($C_5H_{10}O_3$), or acetic acid and butyl acetate ($C_6H_{12}O_2$), all detected in this work (Tables 2 and 3).

(Figure 3)

Other channels could also contribute to the formation of butanoic acid during DBE oxidation, as proposed by Battin-Leclerc et al. [43]: addition of ˙OH to CH_2O yielding to formic acid, reactions of CH_2CO to form acetic acid, and decomposition of cyclic ether's ketohydroperoxides.

(Figure 4)

Hydrogen–Deuterium exchange reactions using D_2O were used to confirm the presence of –OH or –OOH groups in the products (Table 2). An example of the observed H/D exchange for KHPs is given in Figure 4. On can see the increased ratio of $C_8H_{16}DO_4^+$/ $C_8H_{17}O_4^+$. We proceeded similarly to assess the presence of -OH and -OOH groups in other products (Table 2). Thanks to the use of UHPLC-MS-MS with APCI (+) we could separate and characterize the KHP isomers (Fig. 5). Their chemical structure is given in Table 4 and the solvent gradient used here is given in the Supplementary Material (Table S1).

(Figure 5)

Table 4. Chemical structure of fuel radicals and KHPs formed by oxidation of DBE. The most probable KHPs, according to our simulations, are identified by stars (* < ** < ***).

Initial radicals formed by H-atom abstraction on DBE			
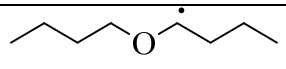	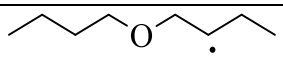	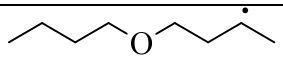	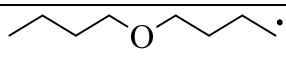
KHPs structure, size of the intermediate in H-atom transfer and C-H bond type (p: primary, s: secondary)			
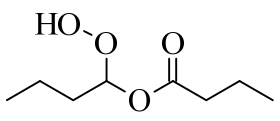	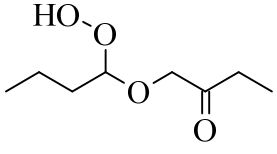	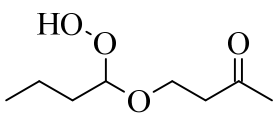	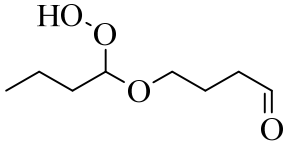

6,s ***	7,s	8,s	9,p
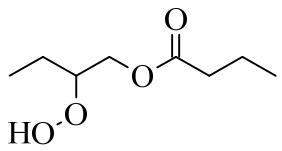	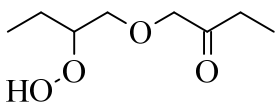	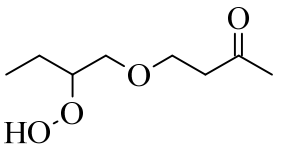	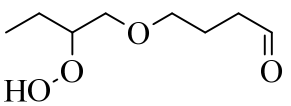
7,s **	8,s	9,s	10,p
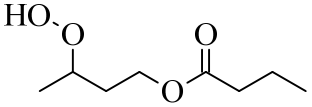	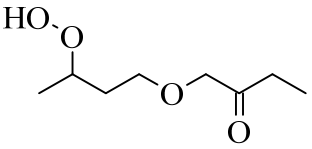	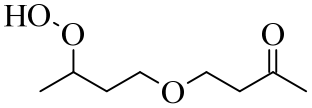	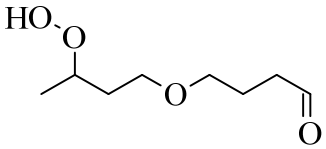
8,s	9,s	10,s	11,p
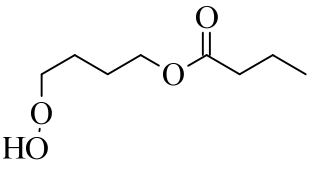	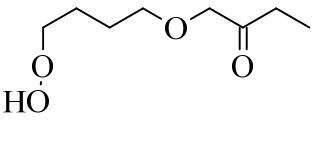	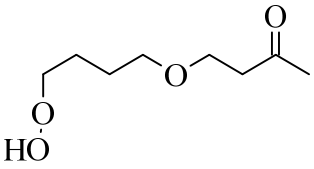	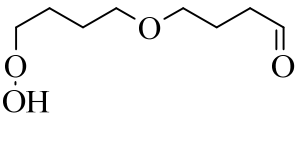
9,s	10,s	11,s	12,p
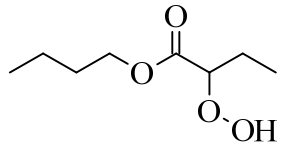	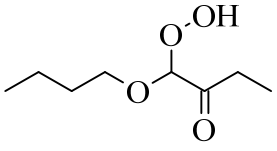	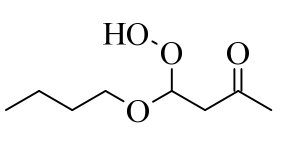	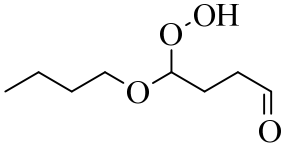
5,s	5,s	6,s	7,p
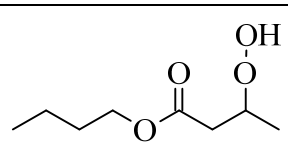	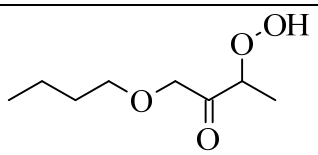	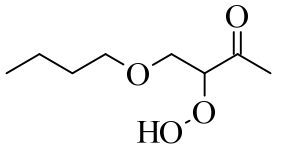	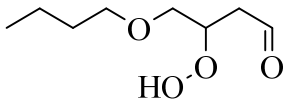
6,s *	5,s	5,s	6,p
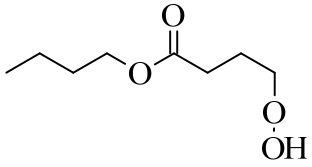	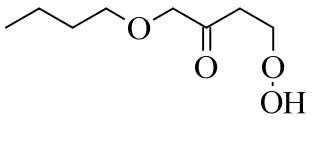	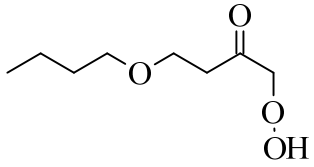	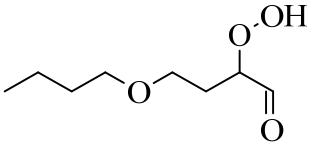
7,s	6,s	5,s	5,p

MS-MS analyses allowed distinguishing two types of isomers: (i) KHPs with hydroperoxyl and carbonyl groups on one side of the ether function and (ii) KHPs with hydroperoxyl and carbonyl groups on both sides of the ether function.

KHPs with both –OOH and –C=O groups on one side of the ether function present a main fragment (100%) m/z 61.0283 ($C_2H_5O_2$) followed by m/z/ 57.0699 (C_4H_9, 25%) and m/z 103.0380 ($C_4H_7O_3$, 30%). These indicate that both -OOH and -C=O groups are on the same side of the ether function. Other fragments at m/z 75.0437, corresponding to a loss of CO (m/z 27.9949) and a fragment m/z 86.0360 corresponding to a loss of HO_2 confirm the global structure of $C_4H_7O_3$.

KHPs with –OOH and –C=O groups both side of the–O- group were identified by a strong m/z 87.0438 (100%) fragment ($C_4H_7O_2$), or m/z 89.0594 (100%) fragment ($C_4H_9O_2$). $C_4H_7O_2$ contains both a -C=O group and an ether function whereas the counterpart $C_4H_9O_2$ contains only an -OOH group. The fragment m/z 71.0490 (C_4H_7O) contains only the -C=O group. The present results indicated that KHPs, and other low-temperature oxidation products, derive from reactions not limited to that of CH_2 groups in α-position to the ether function although H-

atom abstractions are facilitated by weaker C-H bonds (Table 5) near the ether function, as already observed in kinetic studies of a series of ethers + OH reactions [44]. Figure S1 (Supplementary Material) shows the structure of the MS-MS fragments.

Table 5. C-H bond dissociation energies (BDE) in DBE computed using the G3B3 method [45]

Carbon position to -O-	BDE (kcal/mole)
α	95.3
β	100.2
γ	98.8
δ	101.1

To further identify the isomers pertaining to the above delineated two groups of KHPs, their dipole moment was computed [46]. Because of the ACN-water gradient used (from 5 to 90 % ACN) the polarity of the solvent decreases over elution time. Then the more polar KHPs should be eluted first. However, because the computed dipole moments of several KHP are very close relatively large uncertainties arise. Considering an uncertainty of 10% on the calculated dipole moments, we observe that in 75% of the cases the order of elution of the isomers(a-type and b-type) corresponds to that of the dipole moments. The differences are mainly observed at the center of this distribution. Then, it seems risky to propose an identification of KHPs at this stage.

(Figure 6)

Table 3 shows that the present results obtained in a JSR and an RCM show strong similarity. This is further demonstrated in Figure 6 which compares the results of UHPLC-MS analyses (with APCI + for m/z 177.1121) of JSR and RCM samples in the same analytical conditions. The results indicate that the formation of KHPs in both experimental conditions are similar, which should imply the chemistry proceeds similarly in both experimental systems, although the RCM sampling method employed here encompasses many uncertainty sources such as the non- instant freezing of the chemistry during sampling and the non-localized probing. Thus, results are only qualitative.

Our kinetic model was used to simulate the present JSR experiments. Figure 7 shows a comparison of the experimental results (APCI +) and chemical kinetic modeling for DBE and for the sum of KHPs determined under JSR conditions. As can be seen from this figure, the chemical kinetic model well predicts the variation of KHPs concentration as a function of temperature in the cool flame regime.

(Figure 7)

Carboxylic acids are commonly produced in cool flames. For example, formic, acetic, propanoic acid, and butanoic acid were reported by Wang et al. [20] in their study of n- heptane oxidation in a JSR. In the present study, C_2 to C_4 carboxylic acids were detected (Tables 2 and 3), in agreement with previous DBE oxidation studies [9, 10].

(Figure 8)

Cyclic ethers and lactones ($C_8H_{16}O_2$) can be formed during DBE oxidation [9, 10]. They are produced by decomposition of QOOH: QOOH → cyclic ether or lactone + OH. This class of species was observed in the present work (Fig. 8a). Their separation was performed by UHPLC-MS (Fig. S2 and S3 in Supplementary Material). Butyl butyrate was observed at trace level in UHPLC-MS analyses.

The identification of γ-butyrolactone, n-butyl formate, n-butyl acetate, and n-butyl butyrate was done by UHPLC-MS analyses of samples seeded with pure compounds.

Butyric anhydride and di-keto-ethers ($C_8H_{14}O_3$) were detected in the present work (Fig. 8b) whereas only butyric anhydride was reported previously [10]. Diones were observed earlier, e.g., during n -heptane oxidation by Wang et al. [20] in a JSR by SVUV- PIMS and APCI-HRMS. Also, $C_nH_{2n-2}O_2$ (n = 2–6) intermediates which could be C_2–C_6 diones were detected[20]. However, pathways to diones are still uncertain. They could be formed after H-atom abstraction on a KHP and decomposition yielding OH, a dione, and water [47]. UHPLC-MS analyses of

samples spiked with butyric anhydride confirmed its formation. The other isomers could not be identified by UHPLC-MS-MS.

(Figure 9)

C_8 hydroperoxides and C_8 diols ($C_8H_{18}O_3$) can be formed during the low temperature oxidation of DBE. A maximum of 4 ROOH and 16 diols could be produced. No other chemical structure besides hydroperoxides and diols could correspond to $C_8H_{18}O_3$. It is well-known that diols react efficiently with boric acid [48]. Therefore, we successfully tested the formation of esters of boric acid by adding diluted solution of boric acid to the samples. Boric acid mono esters were observed using FIA APCI (+/-) MS analyses (m/z 188.1219 and 205.1246). Bi-cyclic di-esters of boric acid (m/z 331.2292) were formed. More information is given in the Supplementary Material.

OH/OD exchange was used to confirm the presence of $C_8H_{18}O_3$ diols for which a double OH/OD exchange occurs (Table 2).

The separation and detection by UHPLC-MS of $C_8H_{18}O_3$ isomers was performed (Figure 9). MS/MS analyses were performed (Table 6). $C_8H_{18}O_3$ isomers with oxygenated functional groups on one side of the ether function were characterized by MS/MS fragments at m/z 57.0698 (C_4H_9). The distinction between each isomer was made by comparing the relative abundance of the major MS/MS fragments according to the most likely mechanism of formation. The ROOH isomers, where the OOH function is only on one side of the ether function, and all the diol isomers with OH functions on the same side of the ether function, are characterised by a main fragment m/z 57.0698 which corresponds to C_4H_9. Isomers with OH or OOH functions in alpha to the ether function have a major fragment m/z 89.0593 ($C_4H_9O_2$); this is the case for isomers C, E, L, M, and N). The isomers noted A, B, and F with OH or OOH functions at the terminal carbon are characterized by the presence of the specific fragment $C_2H_5O_2$ (m/z 61.0282). When the OH function is in β, γ, or δ of the ether function, we observe the formation of the specific fragment C_3H_7O (m/z 59.0490); this is the case for isomers E, G, H, and J. The absence of this fragment indicates that the OH group is in α position to the ether function (isomer K) or both OH groups are in γ and δ to the ether function (isomer F). Several MS/MS spectra of minor diol isomers with the two OH groups on each side of the ether function show the same fragments with similar relative abundances, which complicates their identification. Therefore 6 isomers could not be fully identified (noted * in Fig. 9).

Table 6: Proposed identification of isomers $C_8H_{18}O_3$ (diols and ROOH)

Isomers structure	RT (min)	Fragments	m/z	relative abundance	comment
A 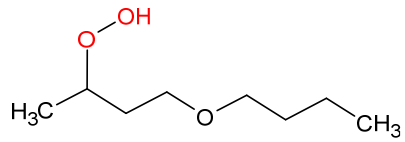	14.49	C_4H_9	57.0698	100 %	
		$C_2H_5O_2$	61.0282	65 %	
		$C_4H_9O_2$	89.0593	30 %	
B 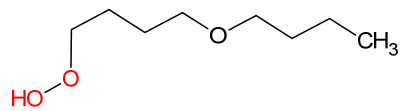	17.53	C_4H_9	57.0698	70 %	
		$C_2H_5O_2$	61.0282	50 %	
		$C_4H_9O_2$	89.0593	35 %	
C 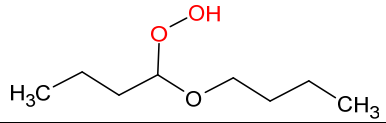	13.32	$C_4H_9O_2$	89.0593	100 %	absence of the $C_2H_5O_2$ fragment
		C_4H_9	57.0698	55 %	
D 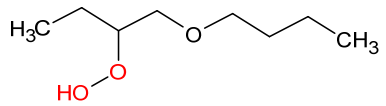	Co-elution with 17.38	C_4H_9	57.0698	70 %	absence of the $C_2H_5O_2$ fragment
		$C_4H_9O_2$	89.0593	55 %	
E 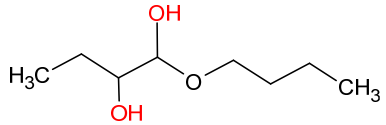	17.38	$C_4H_9O_2$	89.0593	100 %	absence of the $C_2H_5O_2$ fragment
		C_4H_9	57.0698	95 %	
F		C_4H_9	57.0698	100 %	

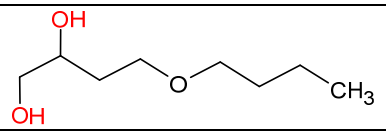	14.80	$C_2H_5O_2$	61.0282	85 %	absence of the C_3H_7O fragment
G 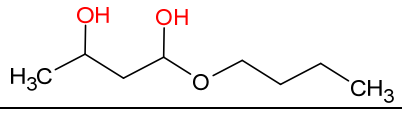	Co-elution with 13.32	C_4H_9	57.0698	100 %	absence of the $C_2H_5O_2$ fragment
		$C_4H_9O_2$	89.0593	45%	
H 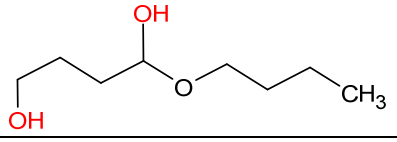	15.07	C_4H_9	57.0698	100 %	absence of the $C_2H_5O_2$ fragment
		$C_4H_9O_2$	89.0593	40 %	
I 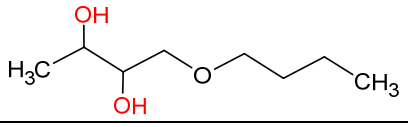	16.55	C_4H_9	57.0698	100 %	absence of the $C_2H_5O_2$ fragment
		$C_4H_9O_2$	89.0593	25 %	
J 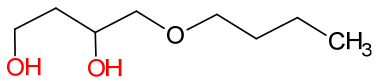	13.61	C_4H_9	57.0698	100 %	absence of the $C_2H_5O_2$ fragment
		$C_4H_9O_2$	89.0593	10 %	
K 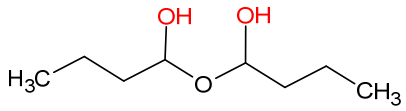	17.62	$C_4H_9O_2$	89.0593	15%	absence of the C_3H_7O fragment
L 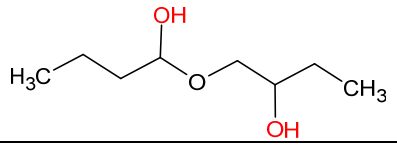	17.15	$C_4H_9O_2$	89.0593	100 %	absence of the C_4H_9 fragment
		C_3H_7O	59.0490	12 %	
M 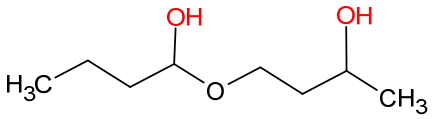	13.04	$C_4H_9O_2$	89.0593	100 %	
		C_3H_7O	59.0490	12 %	
N 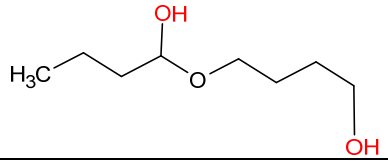	16.43	$C_4H_9O_2$	89.0593	100 %	absence of the C_4H_9 fragment
		C_3H_7O	59.0490	8 %	

Note: The structure of fragments in given in Table S4 (Supplementary Material).

Furthermore, UHPLC-MS/MS analyses of deuterated $C_8H_{18}O_3$ isomers were performed. To this end, water was replaced by D_2O (99.8% D, ref. 756822 from Sigma-Aldrich) in the UHPLC system allowing almost full H/D exchange of the -OH groups. in Figure 10 the peaks of the green chromatogram ($C_8H_{17}D_1O_3$) come from a single OH / OD exchange; they correspond to the ROOHs identified by their MS/MS fragmentation. Likewise, in the red chromatogram, the peaks correspond to diols with double OH/OD exchange ($C_8H_{16}D_2O_3$). These two deuterated ions were not observed when H_2O/ACN was used as mobile phase.

(Figure 10)

Highly oxygenated molecules (MW 190-254) were also observed (Fig. 8). As stated in the first part of this section, they resulted from up to 5 addition of O_2 on fuel's radicals. Among these species, one found di-keto-hydroperoxides (MW 190), di-hydroperoxides (MW 194), keto-di-hydroperoxides (MW 208), di-keto-di-hydroperoxides (MW 222), keto-tri-hydroperoxides (MW 240), and di-keto-tri-hydroperoxides (MW 254). $C_8H_{18}O_5$ (MW 194), $C_8H_{14}O_6$ (MW 206), $C_8H_{16}O_8$ (MW 240), and $C_8H_{14}O_9$ (MW 254) are reported for the first time as products of DBE oxidation whereas the others were reported previously [10]. Here, they were also detected in flow injection analyses and negative ionization mode. The separation of HOMs with formula $C_8H_{16}O_6$ was

performed by UHPLC-MS with some success (Fig. S4 in Supplementary Material) but the analytical method needs to be improved. The solvent gradient used here is given in the Supplementary Material (Table S2). Nevertheless, one could obtain plots showing the variation of HOMs integrated signal as a function of temperature (Fig. 8). The data show some scatter but the trend is that HOMs peak around 550-560 K, which is similar to what was observed for KHPs under the same conditions.

5. Conclusion and Perspectives

The oxidation of di-n-butyl-ether was performed in two experimental systems, namely a jet-stirred reactor and a rapid compression machine. A large range of conditions was considered (1-10 atm, 480-670 K, equivalence ratios of 0.5 and 1). Low-temperature products formed in JSR and RCM experiments were characterized by collecting samples dissolved in acetonitrile and analyzed using a range of techniques (flow injection analyses, UHPLC analyses, high resolution mass spectrometry with HESI +/- and APCI +/-, MS-MS). The RCM sampling method employed here allows only qualitative measurements. Nevertheless, our measurements prove that sampling elusive oxygenated intermediates form RCM facility is possible. Improvement of the sampling protocol is still needed for quantitative measurements. The present analyses allowed characterizing hydroperoxides and diols ($C_8H_{18}O_3$), ketohydroperoxides ($C_8H_{16}O_4$), carboxylic acids ($C_2H_4O_2$, $C_3H_6O_2$, $C_4H_8O_2$), di-keto ethers ($C_8H_{14}O_3$), and highly oxygenated molecules ($C_8H_{14}O_5$, $C_8H_{16}O_6$, $C_8H_{14}O_6$, $C_8H_{14}O_7$, $C_8H_{16}O_8$, and $C_8H_{14}O_9$) resulting from the addition up to five O_2 molecules on fuel's radicals. Also, cyclic ethers and esters were observed. To confirm the presence of –OH or –OOH groups in the oxidation products H/D exchange with D_2O was used. MS-MS analyses indicated the formation of two types of products: KHPs with hydroperoxy and keto groups located (i) on both side of the ether function, or (ii) on one side of the ether function. We attempted to further identify these isomers by using computed dipole moments, but more advanced computations are probably required to reduce uncertainties in products identification. HOMs were detected but more work is needed to identify the different isomers and improve their separation by UHPLC. NMR analyses of the KHPs and HOMs isomers should help finalizing identification. This work is underway. Many of the species newly detected are not included in available reaction schemes for DBE oxidation. Among others, our kinetic reaction mechanism needs to be extended for simulating the formation of newly detected species. The present measurements of low-temperature products performed under JSR and RCM conditions show strong similitude, which indicates common reaction pathways. New experiments performed with IC engines and analyses of the exhaust should be useful to further assess the importance of the chemistry observed in this work.

Acknowledgements

The authors gratefully acknowledge funding from the Labex Caprysses (convention ANR-11-LABX-0006-01) and from the Région Centre Val de Loire, FEDER, and CPER (projects PROMESTOCK and APROPOR-E).

References

[1] K. Yasunaga; F. Gillespie; J. M. Simmie; H. J. Curran; Y. Kuraguchi; H. Hoshikawa; M. Yamane; Y. Hidaka, A Multiple Shock Tube and Chemical Kinetic Modeling Study of Diethyl Ether Pyrolysis and Oxidation, The Journal of Physical Chemistry A 114 (34) (2010) 9098-9109.
[2] F. Gillespie; W. K. Metcalfe; P. Dirrenberger; O. Herbinet; P.-A. Glaude; F. Battin-Leclerc; H. J. Curran, Measurements of flat-flame velocities of diethyl ether in air, Energy 43 (1) (2012) 140-145.
[3] M. Werler; L. R. Cancino; R. Schiessl; U. Maas; C. Schulz; M. Fikri, Ignition delay times of diethyl ether measured in a high-pressure shock tube and a rapid compression machine, Proc. Combust. Inst. 35 (1) (2015) 259-266.
[4] N. Vin; O. Herbinet; F. Battin-Leclerc, Diethyl ether pyrolysis study in a jet-stirred reactor, Journal of Analytical and Applied Pyrolysis 121 (2016) 173-176.
[5] L.-S. Tran; J. Pieper; H.-H. Carstensen; H. Zhao; I. Graf; Y. Ju; F. Qi; K. Kohse-Höinghaus, Experimental and kinetic modeling study of diethyl ether flames, Proceedings of the Combustion Institute 36 (1) (2017) 1165-1173.
[6] Z. Serinyel; M. Lailliau; S. Thion; G. Dayma; P. Dagaut, An experimental chemical kinetic study of the oxidation of diethyl ether in a jet-stirred reactor and comprehensive modeling, Combustion and Flame 193 (2018) 453-462.
[7] Y. Uygun, Ignition studies of undiluted diethyl ether in a high-pressure shock tube, Combustion and Flame 194 (2018) 396-409.
[8] L.-S. Tran; O. Herbinet; Y. Li; J. Wullenkord; M. Zeng; E. Bräuer; F. Qi; K. Kohse-Höinghaus; F. Battin-Leclerc, Low-temperature gas-phase oxidation of diethyl ether: Fuel reactivity and fuel-specific products, Proceedings of the Combustion Institute 37 (1) (2019) 511-519.

[9] S. Thion; C. Togbe; Z. Serinyel; G. Dayma; P. Dagaut, A chemical kinetic study of the oxidation of dibutyl-ether in a jet-stirred reactor, Combust. Flame 185 (2017) 4-15.
[10] L. S. Tran; J. Wullenkord; Y. Y. Li; O. Herbinet; M. R. Zeng; F. Qi; K. Kohse-Hoinghaus; F. Battin-Leclerc, Probing the low-temperature chemistry of di-n-butyl ether: Detection of previously unobserved intermediates, Combust. Flame 210 (2019) 9-24.
[11] O. Perrin; A. Heiss; K. Sahetchian; L. Kerhoas; J. Einhorn, Determination of the isomerization rate constant HOCH2CH2CH2CH(OO center dot)CH3->(HOCHCH2CH2CH)-H-center dot(OOH)CH3. Importance of intramolecular hydroperoxy isomerization in tropospheric chemistry, Int. J. Chem. Kinet. 30 (12) (1998) 875-887.
[12] N. Blin-Simiand; F. Jorand; K. Keller; M. Fiderer; K. Sahetchian, Ketohydroperoxides and ignition delay in internal combustion engines, Combust. Flame 112 (1998) 278-282.
[13] A. Heiss; K. Sahetchian, Isomerization reactions of the n-C4H9O and n-OOC4H8OH radicals in oxygen, Int. J. Chem. Kinet. 28 (7) (1996) 531-544.
[14] K. Sahetchian; J. C. Champoussin; M. Brun; N. Levy; N. Blin-Simiand; C. Aligrot; F. Jorand; M. Socoliuc; A. Heiss; N. Guerassi, Experimental study and modeling of dodecane ignition in a diesel engine, Combust. Flame 103 (3) (1995) 207-220.
[15] M. Zinbo; R. K. Jensen; S. Korcek, Gas-liquid-chromatography of oxygenated compounds related to autoxidation of n-hexadecane, Anal. Lett. 10 (2) (1977) 119-132.
[16] R. K. Jensen; S. Korcek; L. R. Mahoney; M. Zinbo, Liquid-phase autoxidation of organic-compounds at elevated-temperatures .1. stirred flow reactor technique and analysis of primary products from normal-hexadecane autoxidation at 120-degrees-C 180-degrees-C, J. Am. Chem. Soc. 101 (25) (1979) 7574-7584.
[17] R. K. Jensen; S. Korcek; L. R. Mahoney; M. Zinbo, Liquid-phase autoxidation of organic-compounds at elevated-temperatures .2. Kinetics and mechanisms of the formation of cleavage products in normal-hexadecane autoxidation, J. Am. Chem. Soc. 103 (7) (1981) 1742-1749.
[18] R. K. Jensen; M. Zinbo; S. Korcek, HPLC determination of hydroperoxidic products formed in the autoxidation of normal-hexadecane at elevated-temperatures, J. Chromatogr. Sci. 21 (9) (1983) 394-397.
[19] R. K. Jensen; S. Korcek; M. Zinbo, Formation, isomerization, and cyclization reactions of hydroperoxyalkyl radicals in hexadecane autoxidation at 160-190-degrees-C, J. Am. Chem. Soc. 114 (20) (1992) 7742-7748.
[20] Z. D. Wang; B. J. Chen; K. Moshammer; D. M. Popolan-Vaida; S. Sioud; V. S. B. Shankar; D. Vuilleumier; T. Tao; L. Ruwe; E. Brauer; N. Hansen; P. Dagaut; K. Kohse-Hoinghaus; M. A. Raji; S. M. Sarathy, n-Heptane cool flame chemistry: Unraveling intermediate species measured in a stirred reactor and motored engine, Combust. Flame 187 (2018) 199-216.
[21] Z. Wang; D. M. Popolan-Vaida; B. Chen; K. Moshammer; S. Y. Mohamed; H. Wang; S. Sioud; M. A. Raji; K. Kohse-Höinghaus; N. Hansen; P. Dagaut; S. R. Leone; S. M. Sarathy, Unraveling the structure and chemical mechanisms of highly oxygenated intermediates in oxidation of organic compounds, Proceedings of the National Academy of Sciences 114 (50) (2017) 13102-13107.
[22] F. Bianchi; T. Kurtén; M. Riva; C. Mohr; M. P. Rissanen; P. Roldin; T. Berndt; J. D. Crounse; P. O. Wennberg; T. F. Mentel; J. Wildt; H. Junninen; T. Jokinen; M. Kulmala; D. R. Worsnop; J. A. Thornton; N. Donahue; H. G. Kjaergaard; M. Ehn, Highly Oxygenated Organic Molecules (HOM) from Gas-Phase Autoxidation Involving Peroxy Radicals: A Key Contributor to Atmospheric Aerosol, Chemical Reviews 119 (6) (2019) 3472-3509.
[23] K. Moshammer; A. W. Jasper; D. M. Popolan-Vaida; A. Lucassen; P. Dievart; H. Selim; A. J. Eskola; C. A. Taatjes; S. R. Leone; S. M. Sarathy; Y. G. Ju; P. Dagaut; K. Kohse-Hoinghaus; N. Hansen, Detection and Identification of the Keto-Hydroperoxide (HOOCH2OCHO) and Other Intermediates during Low-Temperature Oxidation of Dimethyl Ether, J. Phys. Chem. A 119 (28) (2015) 7361-7374.
[24] K. Moshammer; A. W. Jasper; D. M. Popolan-Vaida; Z. D. Wang; V. S. B. Shankar; L. Ruwe; C. A. Taatjes; P. Dagaut; N. Hansen, Quantification of the Keto-Hydroperoxide (HOOCH2OCHO) and Other Elusive Intermediates during Low-Temperature Oxidation of Dimethyl Ether, J. Phys. Chem. A 120 (40) (2016) 7890-7901.
[25] P. Dagaut; N. Belhadj; R. Benoit; G. Dayma; M. Lailliau; Z. Serinyel, in: *MCS11 11th Mediterranean Combustion Symposium* https://hal.archives-ouvertes.fr/hal-02137413, Tenerife, Spain, 2019.
[26] P. Dagaut; M. Cathonnet; J. P. Rouan; R. Foulatier; A. Quilgars; J. C. Boettner; F. Gaillard; H. James, A Jet-Stirred Reactor for Kinetic-Studies of Homogeneous Gas-Phase Reactions at Pressures up to 10-Atmospheres (~ 1 MPa), Journal of Physics E-Scientific Instruments 19 (3) (1986) 207-209.
[27] P. Dagaut; M. Cathonnet; J. C. Boettner; F. Gaillard, Kinetic modeling of ethylene oxidation, Combust. Flame 71 (3) (1988) 295-312.
[28] G. Dayma; K. Hadj Ali; P. Dagaut, Experimental and detailed kinetic modeling study of the high pressure oxidation of methanol sensitized by nitric oxide and nitrogen dioxide, Proc. Combust. Inst. 31 (1) (2007) 411-418.

[29] M. Y. Wang; K. W. Zhang; G. Kukkadapu; S. W. Wagnon; M. Mehl; W. J. Pitz; C. J. Sung, Autoignition of trans-decalin, a diesel surrogate compound: Rapid compression machine experiments and chemical kinetic modeling, Combust. Flame 194 (2018) 152-163.
[30] L. Yu; Z. Wu; Y. Qiu; Y. Qian; Y. Mao; X. Lu, Ignition delay times of decalin over low-to-intermediate temperature ranges: Rapid compression machine measurement and modeling study, Combust. Flame 196 (2018) 160-173.
[31] K. Alexandrino; M. U. Alzueta; H. J. Curran, An experimental and modeling study of the ignition of dimethyl carbonate in shock tubes and rapid compression machine, Combust. Flame 188 (2018) 212-226.
[32] N. Bourgeois; S. S. Goldsborough; G. Vanhove; M. Duponcheel; H. Jeanmart; F. Contino, CFD simulations of Rapid Compression Machines using detailed chemistry: Impact of multi-dimensional effects on the auto-ignition of the iso-octane, Proc. Combust. Inst. 36 (1) (2017) 383-391.
[33] M. D. Le; M. Matrat; A. Ben Amara; F. Foucher; B. Moreau; Y. Yu; P.-A. Glaude, in: *14th International Conference on Engines & Vehicles*, SAE International: 2019; pp SAE Technical Paper 2019-24-0069
[34] M. Pochet; V. Dias; B. Moreau; F. Foucher; H. Jeanmart; F. Contino, Experimental and numerical study, under LTC conditions, of ammonia ignition delay with and without hydrogen addition, Proc. Combust. Inst. 37 (1) (2019) 621-629.
[35] C. J. Sung; H. J. Curran, Using rapid compression machines for chemical kinetics studies, Prog. Energy Combust. Sci. 44 (2014) 1-18.
[36] S. P. Pasilis; V. Kertesz; G. J. Van Berkel, Unexpected analyte oxidation during desorption electrospray ionization-mass spectrometry, Anal. Chem. 80 (4) (2008) 1208-1214.
[37] M. Chen; K. D. Cook, Oxidation artifacts in the electrospray mass spectrometry of A beta peptide, Anal. Chem. 79 (5) (2007) 2031-2036.
[38] P. Glarborg; R. J. Kee; J. F. Grcar; J. A. Miller in: *PSR: A FORTRAN program for modeling well-stirred reactors.*, SAND86-8209, Sandia National Laboratories, Livermore, CA, 1986
[39] R. J. Kee; F. M. Rupley; J. A. Miller in: *CHEMKIN-II: A Fortran Chemical Kinetics Package for the Analysis of Gas-Phase Chemical Kinetics.*, SAND89-8009, Sandia National Laboratories, Livermore, CA, 1989
[40] A. Jalan; I. M. Alecu; R. Meana-Paneda; J. Aguilera-Iparraguirre; K. R. Yang; S. S. Merchant; D. G. Truhlar; W. H. Green, New Pathways for Formation of Acids and Carbonyl Products in Low-Temperature Oxidation: The Korcek Decomposition of gamma-Ketohydroperoxides, J. Am. Chem. Soc. 135 (30) (2013) 11100-11114.
[41] Z. D. Wang; S. M. Sarathy, Third O-2 addition reactions promote the low-temperature auto-ignition of n-alkanes, Combust. Flame 165 (2016) 364-372.
[42] C. A. Grambow; A. Jamal; Y. P. Li; W. H. Green; J. Zador; Y. V. Suleimanov, Unimolecular Reaction Pathways of a gamma-Ketohydroperoxide from Combined Application of Automated Reaction Discovery Methods, J. Am. Chem. Soc. 140 (3) (2018) 1035-1048.
[43] F. Battin-Leclerc; A. A. Konnov; J. L. Jaffrezo; M. Legrand, To better understand the formation of short-chain acids in combustion systems, Combust. Sci. Technol. 180 (2) (2008) 343-370.
[44] T. J. Wallington; P. Dagaut; R. Z. Liu; M. J. Kurylo, Rate Constants for the Gas-Phase Reactions of OH with C-5 through C-7 Aliphatic-Alcohols and Ethers - Predicted and Experimental Values, Int. J. Chem. Kinet. 20 (7) (1988) 541-547.
[45] M. J. Frisch; G. W. Trucks; H. B. Schlegel; G. E. Scuseria; M. A. Robb; J. R. Cheeseman; G. Scalmani; V. Barone; B. Mennucci; G. A. Petersson; H. Nakatsuji; M. Caricato; X. Li; H. P. Hratchian; A. F. Izmaylov; J. Bloino; G. Zheng; J. L. Sonnenberg; M. Hada; M. Ehara; K. Toyota; R. Fukuda; J. Hasegawa; M. Ishida; T. Nakajima; Y. Honda; O. Kitao; H. Nakai; T. Vreven; J. J. A. Montgomery; J. E. Peralta; F. Ogliaro; M. Bearpark; J. J. Heyd; E. Brothers; K. N. Kudin; V. N. Staroverov; R. Kobayashi; J. Normand; K. Raghavachari; A. Rendell; J. C. Burant; S. S. Iyengar; J. Tomasi; M. Cossi; N. Rega; J. M. Millam; M. Klene; J. E. Knox; J. B. Cross; V. Bakken; C. Adamo; J. Jaramillo; R. Gomperts; R. E. Stratmann; O. Yazyev; A. J. Austin; R. Cammi; C. Pomelli; J. W. Ochterski; R. L. Martin; K. Morokuma; V. G. Zakrzewski; G. A. Voth; P. Salvador; J. J. Dannenberg; S. Dapprich; A. D. Daniels; Ö. Farkas; J. B. Foresman; J. V. Ortiz; J. Cioslowski; D. J. Fox, in: Gaussian, Inc.: Wallingford CT, 2009.
[46] J. Gasteiger; M. Marsili, A new model for calculating atomic charges in molecules, Tetrahedron Lett. 19 (34) (1978) 3181-3184.
[47] E. Ranzi; C. Cavallotti; A. Cuoci; A. Frassoldati; M. Pelucchi; T. Faravelli, New reaction classes in the kinetic modeling of low temperature oxidation of n-alkanes, Combust. Flame 162 (5) (2015) 1679-1691.
[48] S. Z. Ackloo; P. C. Burgers; B. E. McCarry; J. K. Terlouw, Structural analysis of diols by electrospray mass spectrometry on boric acid complexes, Rapid Commun. Mass Spectrom. 13 (23) (1999) 2406-2415.

Figures

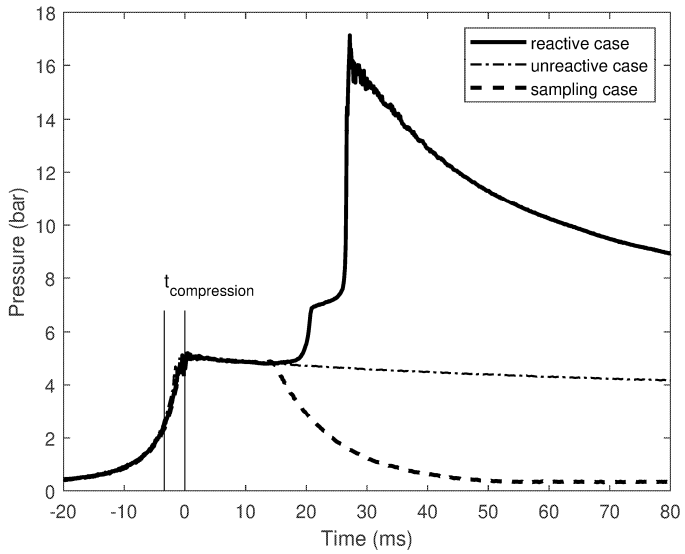

Figure 1. Pressure histories of three RCM tests (reactive, unreactive, and sampling case). P_c = 5 bar, T_c=555 K, φ = 1.

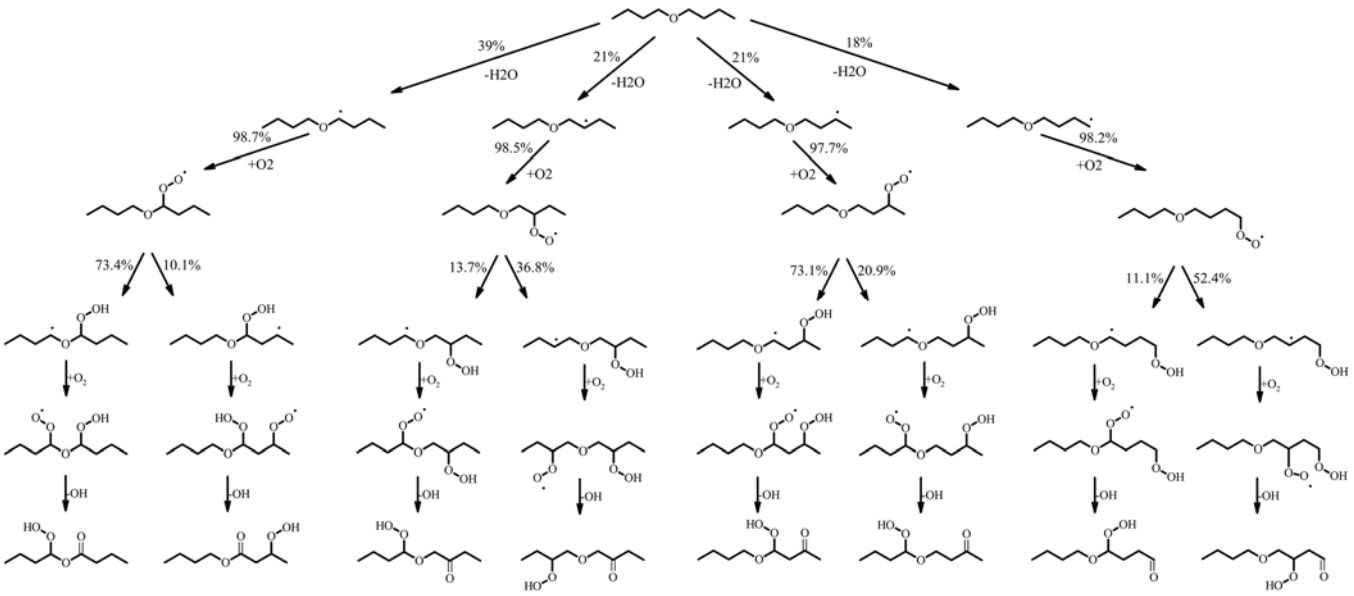

Figure 2. Computed oxidation pathways for DBE (5000 ppm, 10 atm, 1 s residence time, φ = 0.5).

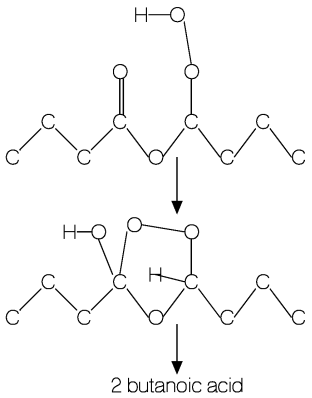

Figure 3. Formation of butanoic acid through the decomposition di-n-butyl ether γ-ketohydroperoxide, according to the so-called Korcek mechanism.

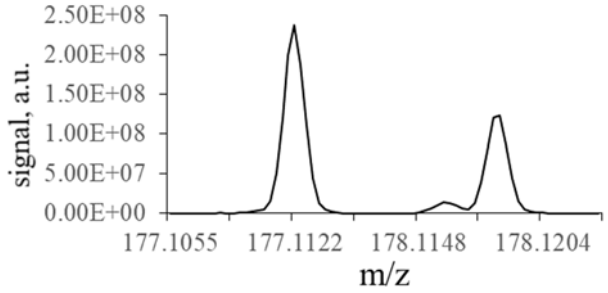

Figure 4. Mass spectrum showing the increased ratio $C_8H_{16}DO_4^+$/ $C_8H_{17}O_4^+$ due to OH/OD exchange on KHPs. No signal at m/z 178.1184 was recorded without addition of D_2O. Analyses were performed in HESI positive mode. The little signal at m/z 178.116 corresponds to $C_7{}^{13}CH_{17}O_4$.

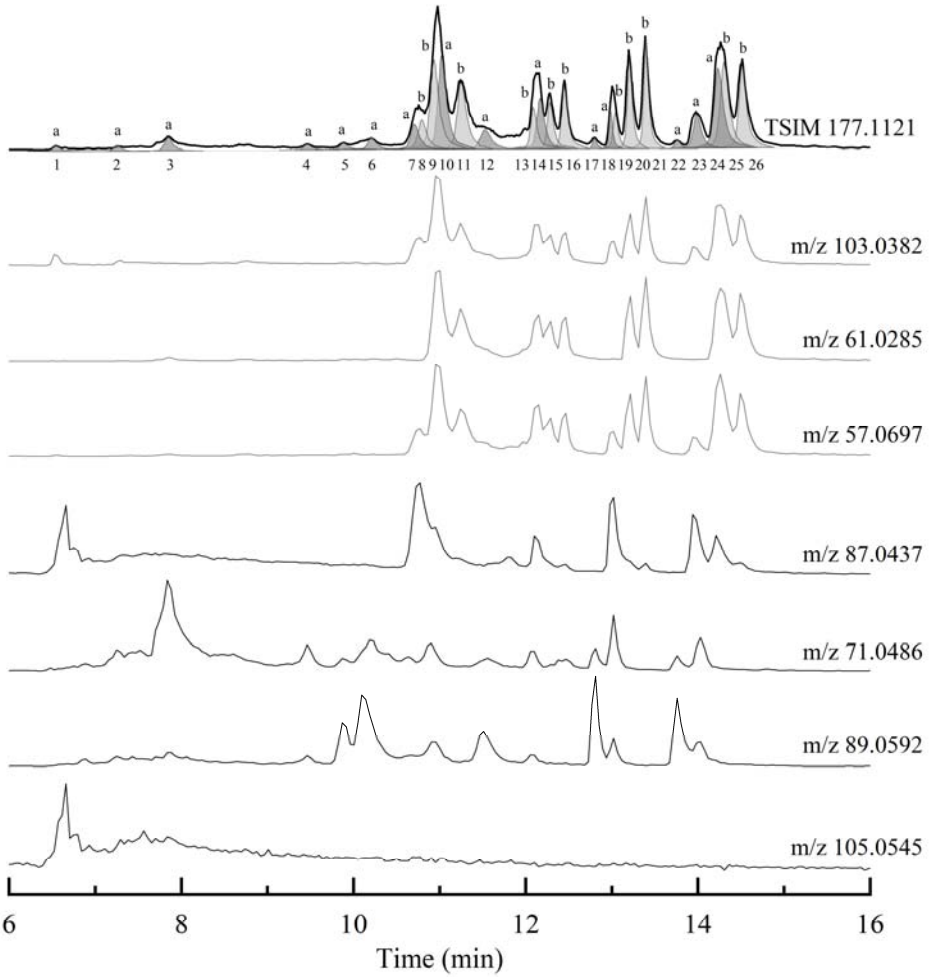

Figure 5. Typical chromatogram obtained for m/z 177.1121 (APCI +). KHPs with -OOH and -C=O on both sides of the ether function (a) and on one side (b) are indicated. The structure of the isomers is given in Table 4.

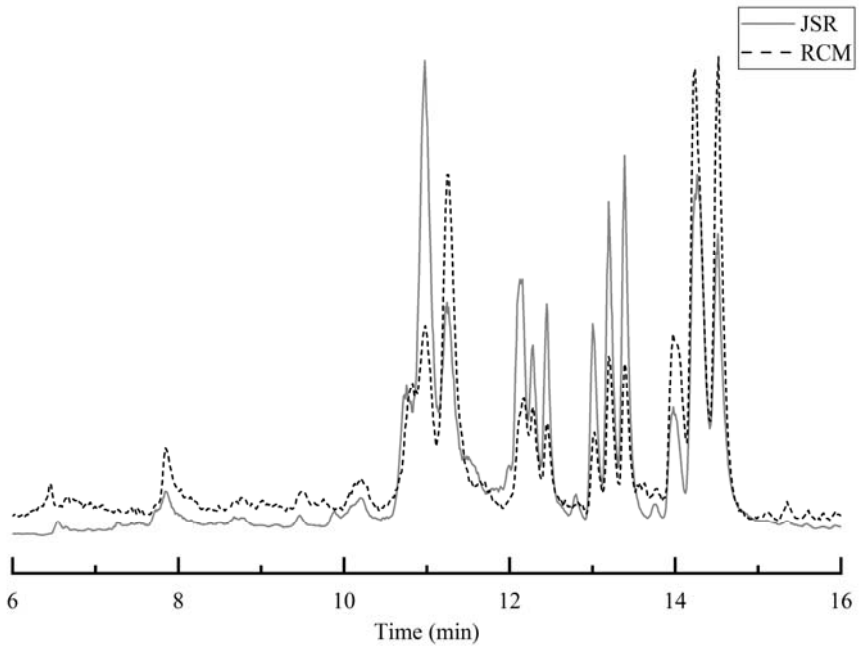

Figure 6. UHPLC analysis of KHPs. Comparison of chromatographic traces obtained with samples obtained by oxidation of DBE in a JSR (1 atm, 520 K) and an RCM (5 bar, 553 K).

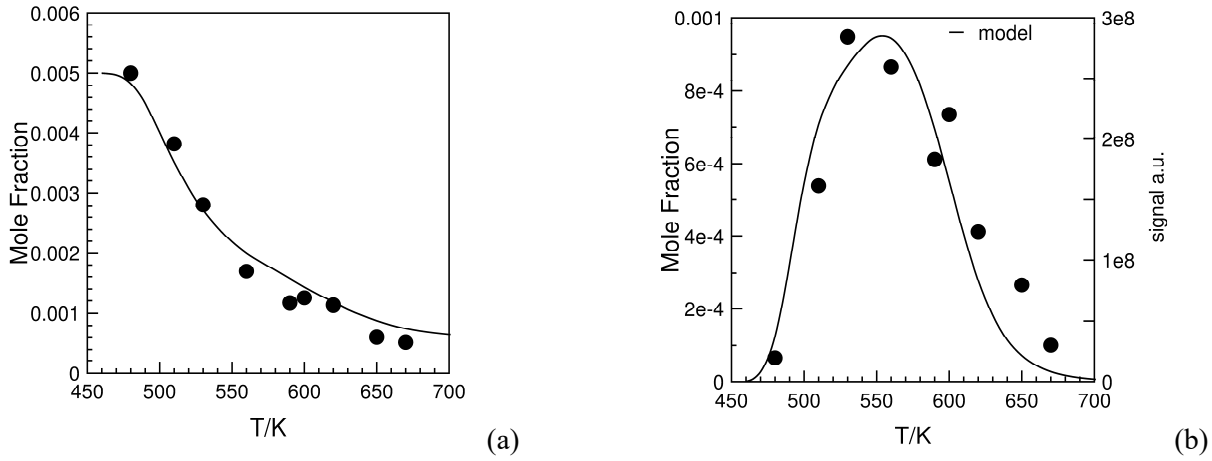

Figure 7. Comparison between experimental data (symbols) and modeling (line) for the oxidation of 5000 ppm of DBE (φ = 0.5, residence time of 1 s, and 10 atm). (a) Consumption of DBE. (b) Formation of KHPs: the data were obtained by integration of UHPLC-MS signal and scaled to the computed maximum experimental concentration. Experimental errors are estimated to be of the order of 40%.

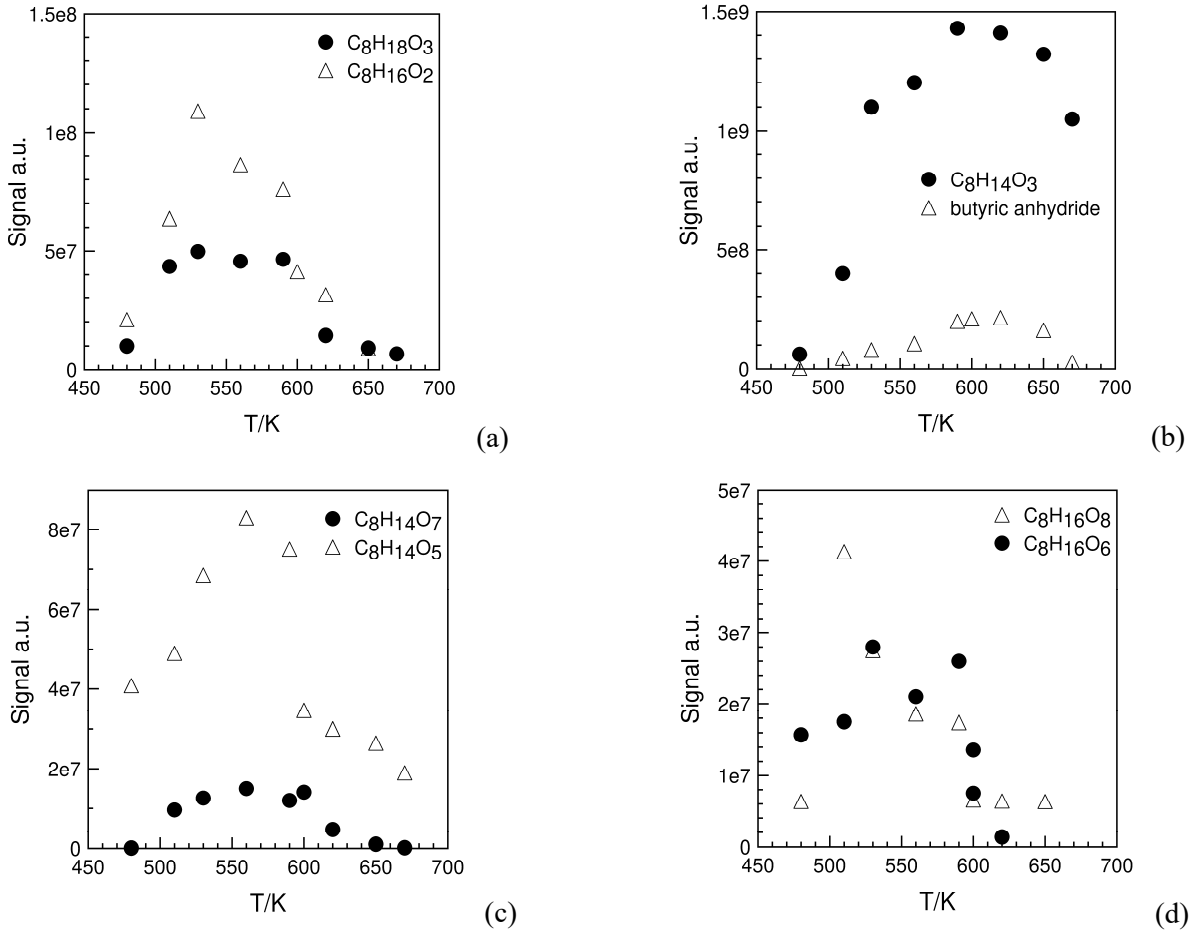

Figure 8. HOMs formation by oxidation of DBE in a JSR at 10 atm obtained as a function of temperature. Experimental errors are estimated to be of the order of 40%. (a) $C_8H_{16}O_2$: Cyclic ethers and butyl butyrate (FIA, m/z 145.1222, APCI+); $C_8H_{18}O_3$: ROOH and diols (UHPLC, m/z 163.1327, APCI+); (b) $C_8H_{14}O_3$: di-keto-ethers including butyric anhydride (UHPLC, m/z 159.1016, APCI+); (c) $C_8H_{14}O_5$: di-keto-ROOH (FIA, m/z 191.0914, APCI+); $C_8H_{14}O_7$: di-keto-di-ROOH (UHPLC, m/z 223.0812, APCI+); (d) $C_8H_{16}O_6$: keto-di-ROOH (FIA, m/z 207.0873, APCI -), $C_8H_{16}O_8$ keto-tri-ROOH (FIA, m/z 239.0773, APCI-).

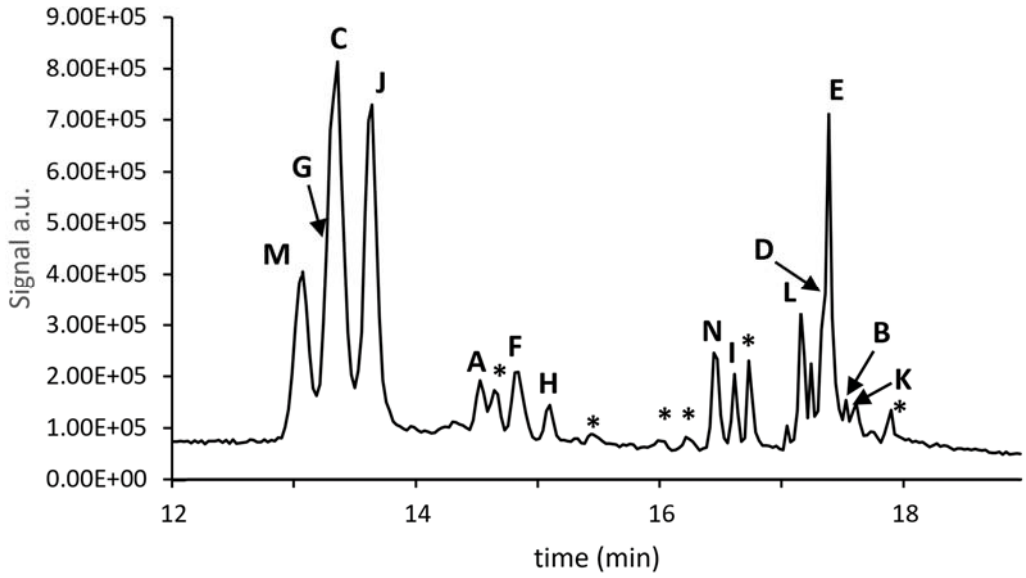

Figure 9. $C_8H_{18}O_3$ formation. Chromatographic trace obtained from the oxidation of DBE in a JSR at 1 atm and 520 K and UHPLC-MS analyses (APCI +, m/z 163.1327). Asterisks indicate diols which could not be identified. The letters refer to Table 6 where the structure of isomers is given.

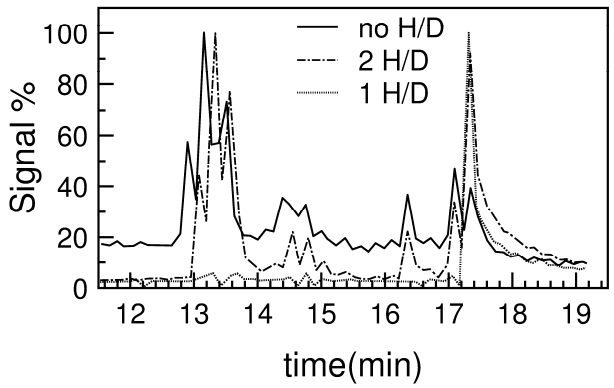

Figure 10. UHPLC-MS/MS (APCI +) analyses of samples of DBE oxidation. D_2O/ACN was used as mobile phase in chromatograms shown as dashed and dotted lines whereas the same gradient using water/ACN was used to obtain the continuous line chromatogram.